



Carbon dioxide-assisted thermochemical conversion of magnetically harvested harmful algae into syngas and metal biochar

Hyeonjung Yu^a, Jeong-Yun Jang^a, In-Hyun Nam^a, Hwanju Jo^a, Gil-Jae Yim^a, Hocheol Song^b, Dong-Wan Cho^{a,*}

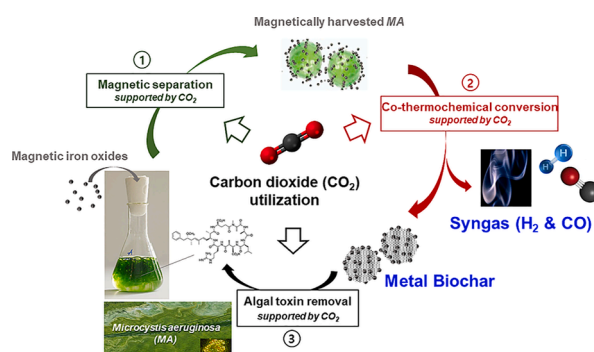
^a Mineral Resources Division, Korea Institute of Geoscience and Mineral Resources (KIGAM), Daejeon 34132, Republic of Korea

^b Department of Earth Resources and Environmental Engineering, Hanyang University, Seoul 04763, Republic of Korea

HIGHLIGHTS

- Efficient algae harvesting using magnetic iron oxides after CO₂ purging.
- CO₂-supported co-pyrolysis of magnetically harvested algae.
- Increased syngas generation through phase transition of iron oxides.
- Thermochemical conversion of CO₂ into CO by oxygen-deficient iron oxides.
- Low level of toxin by addition of metal-biochar into CO₂-purged algal solution.

GRAPHICAL ABSTRACT



ARTICLE INFO

Keywords:

Carbon dioxide-assisted co-pyrolysis
Metal-biochar
Microcystis aeruginosa
Microcystin
Syngas generation

ABSTRACT

With rising of harmful algae blooming and toxin exposure, practical utilization of harmful algae has been developed. This work aimed to magnetically harvest *Microcystis aeruginosa* (MA) using iron oxides and investigate the feasibility of algae/iron oxides mixture as feedstock in pyrolytic platform to produce syngas and metal biochar. Carbon dioxide (CO₂) was used as a feeding gas to enhance the production efficiency of syngas and also functioned pH controller for better MA harvesting and toxin removal. CO₂ support brought multiple benefits: magnetite (Fe₃O₄) and maghemite (γ-Fe₂O₃) recovered MA in a relatively short period of time (~1 min), the recovered biomass generated 34-fold increased carbon monoxide, and metal biochar adsorbed higher amount of toxin from MA (2.8-fold). Pyrolytic utilization of harmful algae supported by CO₂ and iron oxides could be one of promising techniques for evolution of metal biochar to remove toxin, while efficiently recover biomass and enhance syngas production.

* Corresponding author at: 124, Gwahak-ro, Yuseong-gu, Daejeon, Republic of Korea.

E-mail address: dwcho@kigam.re.kr (D.-W. Cho).

1. Introduction

A severe eutrophication triggered by increase of nutrient loads and the global warming has caused 'algal-bloom' problem such as ecosystem destruction, negative tastes/odors-inducing matters, and algal toxins emission over the worlds. The excessive exposure to the harmful toxins may also threaten the human health by neurologically attacking liver, kidney, respiratory system etc. (Zhang et al., 2021). Among the harmful algal species, *Microcystis aeruginosa* is dominantly found in eutrophic lake or river during the summer season and releases the toxin 'microcystin' into the aquatic environment.

It is highly desired to reliably remove or recover the harmful algae species from aquatic system. In general, many techniques has been investigated for harvesting of algal biomass, such as centrifugation, flocculation, flotation and filtration (Li et al., 2021; Singh & Patidar, 2018). However, finding an algae recovery option in the efficient way is still challenging due to the limitation of existing methods such as high cost for operation, energy-intensive, time-consuming or possibility of other contamination by added materials. Recently, magnetic separation using solid minerals (e.g., magnetic iron oxides) has shown the outstanding recovery of algae species (>90% removal within 1–5 min) owing to electrostatic interactions between the oxide surfaces and algal cells (Vasistha et al., 2021). In addition, less adverse effects of magnetic iron oxides addition on water conditions for algal cultivation were found (Markeb et al., 2019), which further encouraged magnetic harvesting of algae species in water. On the other hands, the harvested algal biomass has been widely utilized as a feedstock for producing valuable products (e.g., biodiesel, biohydrogen, bioethanol, biomethane, syngas etc.) through diverse biochemical technologies such as algal biorefinery or fermentation processes (Chen et al., 2023). However, they still have several drawbacks with high costs, long reaction time, complicated processes (Amin et al., 2022; Ayub et al., 2022). In addition, the exposure of algal toxin must be considered for utilization of harmful algae based products. On the other hands, thermochemical conversion processes, especially for the pyrolysis/gasification process, have great potential as feasible option due to the relatively short reaction time, generation of useful products from dynamic and complex wastes with minimal residues (Choudhary et al., 2022; Mokhta et al., 2020). In general, thermochemical conversion takes place in an inert gas and creates valuable products including biochar, bio-oil and syngas (carbon monoxide (CO) & hydrogen (H₂)). Biochar commonly contains well-formed porous structure with high surface area and various functional groups which are favorable for environmental remediation (Ambaye et al., 2021; Cheng et al., 2021; Hadiya et al., 2022). Bio-oil and syngas have been supposed as eco-friendly substitutes for scarce conventional fossil fuels (Seo et al., 2022). Therefore, utilization of harmful algal biomass as a feedstock for pyrolytic process can be a proper technique for treating wastes and generating valuable products, even in industrial application for simple and easy operation.

Nevertheless, thermochemical process still need to be developed for more robust application. Previous studies co-pyrolyzed transition metal or metal oxide nanoparticles with biochar in order to enhance physicochemical properties. These metal biochar can overcome the limitation in adsorptive function of pristine biochar with relatively higher surface area, and better removal ability for pollutants, such as dyes (methylene blue, methyl orange), heavy metals [Pb(II), As(III, V), U(VI)], and nitrogen-containing ions (NH₄⁺, NO₃⁻) (Weidner et al., 2022; Zhao et al., 2021). As a series of enhancing the efficiency of pyrolytic process, reacting CO₂ with biomass feedstocks during pyrolysis has been considered. Feeding CO₂ into the thermochemical reactor altered the properties of biochar so that highly porous framework could be formed in its matrix due to micropores development (Foong et al., 2021), and the structure of biochar contained higher stability to the aging process or surface oxidation than that of N₂ (Kim et al., 2021; Kim et al., 2019). Furthermore, syngas production from thermal cracking of biomass has been outstandingly increased owing to the reaction between volatile

organic compounds (VOCs) from the biomass and CO₂ (Kim et al., 2019). Purging of CO₂ gas to the microalgal culture, commonly having alkaline condition created by sufficient algal growth, can supply CO₂ for microalgal growth and develop efficient biomass harvesting using magnetic particles by decreasing the medium pH (Li et al., 2020). The solution pH has been widely examined as a significant factor in biochar-based treatment, and the control of pH below neutral point (<7) was favored to the adsorptive removal of pollutants by biochar (Yaashikaa et al., 2019).

The demands of applicable utilization of CO₂ and harmful algae biomass for renewable and sustainable technologies has been increasing respectively, but there were few researches to develop interlinked process for solving both of them. Therefore, the use of CO₂ as pH controller and reaction medium was examined. In addition, the feasibility of magnetically harvested *Microcystis aeruginosa* was investigated as feedstock in pyrolytic platform to produce syngas (H₂ & CO) and metal biochar. Among magnetic iron oxides, maghemite (γ-Fe₂O₃) and magnetite (Fe₃O₄) were tested as algal separator and pyrolysis-enhancing medium for dual purpose. Therefore, the potential of CO₂ for supporting biomass harvesting, syngas production and toxin removal were examined in an integrated manner.

2. Materials and methods

2.1. Preparation of algae

A harmful algae, *Microcystis aeruginosa* FBCC-A68 (MA) was provided from Freshwater Bioresources Culture Collection (FBCC) of Nakdonggang National Institute of Biological Resources (NNIBR), South Korea. The algal solution was cultured at a ratio of 10–20% (v/v) in the BG-11 medium (C3061, Sigma-Aldrich, USA), which was sterilized by means of autoclaving at 121 °C for 15 min. The cultures used 500 mL of Duran bottle as a reactor with hose connection cap for air purging. The algal cultivation was conducted in the growth chamber, located in Daejeon (HB-301 M-3, Hanbaek Science co., South Korea). Temperature of the chamber was maintained at 28 °C, and 30% of relative humidity was given under 3 side of fluorescent lamp (3000±500 lx). The photoperiod cycle was set up at 12-h light-on and 12-h light-off (dark) in one day. The algae species were subcultured repeatedly every one week at a same ratio of 20% (v/v) for 10 cycles. The algal growth was determined by optical density value (AquaPen-C AP 110-C, Czech Republic) and microscopic analysis (Primostar 3, ZEISS, Germany). After repetitive obvious algal growth, the culture was cultivated in a 1 L reactor with same condition as mentioned. Each reactor was aerated with filtered ambient air (filter pore size: 0.22 μm, 250 mL min⁻¹), and the algal biomass was harvested when the optical density reached at 1.0.

2.2. Algae harvesting using iron oxides

Harvesting of microalgal biomass was tested using two types of iron oxides, maghemite (γ-Fe₂O₃, <50 nm, Sigma-Aldrich, USA) and magnetite (Fe₃O₄, 50–100 nm, Sigma-Aldrich, USA). Three different types of samples were prepared to compare the efficiency of harvesting within the same period of time; only microalgal biomass (MA), MA/maghemite mixture (MAMH), and MA/magnetite mixture (MAMN). The amount of MA was fixed at 1 g, and the mixing mass ratio of iron oxides to MA was 1. For the case of harvesting without any medium, the biomass was centrifuged at 1,600 g for 15 min. On the other hand, harvesting tests of iron oxides were carried out by adding iron oxides into algal solutions with or without CO₂ gas (200 mL min⁻¹) purging for 5 min. Then, the metal-coupled biomass was collected during 1 min using magnetic field of neodymium magnet. Each of harvested biomass was placed on the 7-cm alumina crucible, dried for 24 h at a temperature of 105 °C, and stored in the desiccator at room temperature.

2.3. Co-pyrolysis of algae/iron oxides mixture

The samples were put on the center of quartz tube of the pyrolysis furnace (tube diameter: 8 cm and tube length: 100 cm), located in Daejeon (SH Scientific, South Korea) with controller measuring the internal temperature. Three different types of gas were used for the creation of atmospheric environment according to the requirements; ultra-high purity of N₂ and CO₂ gases ($\geq 99.999\%$), and 20% CO₂ balanced with nitrogen gas (Daesung Gas co., South Korea). The pyrolytic temperature was increased at a heating rate of 10 °C min⁻¹, from 200 °C to 450, 550 or 650 °C and maintained at final temperature for 30 min. The flow rate of atmospheric gases was set at 220 mL min⁻¹.

2.4. Analytic methods for pyrolytic products

The effluent gases were measured using a micro-gas chromatography (Agilent 490 Micro-GC, Agilent Technologies, Inc., USA) connected with furnace in real-time for monitoring the gas production during the pyrolytic process. The morphology and elemental composition of surface of biochar were analyzed by a field emission scanning electron microscope with energy dispersive x-ray spectroscopy (FE-SEM, TESCAN, CLARA, Czech Republic; EDS, OXFORD, Ultim Max, United Kingdom). The surface shapes of samples were obtained at diverse magnification and acceleration voltage. The surface area and pore size distribution were characterized with N₂ adsorption/desorption isotherm using a Brunauer-Emmett-Teller (BET) surface analyzer (ASAP2420 Micrometrics, Japan). X-ray diffractometer (XRD, X-Pert PRO MPD X-ray diffractometer, Japan) was utilized for detecting the mineral phases of biochar and Raman spectra were recorded (LabRAM HR-800 UV-Visible-NIR, Horiba Jobin Yvon, Japan) with laser line of 514 nm and the spectral range from 800 to 2000 cm⁻¹ to evaluate the degree of graphitization of the biochar. All the equipment used in this study was located in Daejeon, South Korea.

2.5. Microcystin adsorption test

The MA culture was cultivated for two weeks, same condition as prepared the biomass, to test if the produced biochar facilitated the adsorptive removal of microcystin from algal culture in this study. To mimic the environmental field, not the microcystin standard solution as previous researches used (Zhan & Hong, 2022), but the culture contained microcystin exposed from MA, and MA biomass was used for conducting adsorption test. The cultivated solution was sonicated at 40 kHz for 10 min (UCP-02, Lab companion, South Korea) for destroying cell wall of MA to increase the concentration of microcystin. The sonicated solution was purged using ultra-pure CO₂ gas (200 mL min⁻¹) during 5 min for making acidic solution condition, or without purging system was run in parallel for comparison. Each of biochar (MA, MAMH, MAMN) concentration was 1 g/L, and the working volume of adsorption test was 20 mL. After then, all the prepared sample was mixed at 60 rpm for 1 day (24 h), and the sample was filtered using 0.2 µm PTFE syringe filter. Microcystin concentration was measured by high-performance liquid chromatography (HPLC; Waters515, Waters, USA) with photodiode array detection system (PDA), as described by Kim et al. (2018). The 180 µL of filtrated samples were injected into C₁₈ column, and the mobile phase combined 42% of acetonitrile with 0.1% of trifluoroacetic acid was flowed at 0.3 mL min⁻¹. The separated peak from HPLC column was determined by UV detector at 238 nm.

3. Results and discussion

3.1. CO₂-supported harvesting of biomass using iron oxides

For the practical application of microalgal biomass, the efficient biomass harvesting process should precede the pyrolytic process. In this work, the harvesting efficiencies of adding magnetic iron oxides (MN &

MH) into the algal solutions were tested, and the feasibility of CO₂ purging to boost the harvesting was also examined. As shown in Table 1, only 3% algal biomass was recovered on gravity (auto-settling) during 3 min, showing that the biomass could not easily collected without any treatments. There was no distinct difference in harvesting efficiency between MN & MH. In addition, the low level of biomass harvesting (14.1–17.6%) was appeared in the presence of iron oxides regardless of agitation time (~30 min). These observations could be related to the alkaline pH condition of algal solution. The algae growth for two weeks rendered the medium pH highly alkaline (pH 9.4) by consuming CO₂ through photosynthesis, which might hinder aggregation of two different particles (algae & iron oxides) present in solution. Considering that the negative charge density of algae species is generally high within the wide pH range (4–12) and the surface of iron oxides becomes negatively charged above pH 6.5 (Geada et al., 2019), electrostatic repulsion can occur between two different surfaces at this experimental condition. In addition, negative zeta potential of two iron oxides (-17.1 at pH 9.04 for MH, -14.2 at pH 8.93 for MN) can support the low efficiency under the alkaline condition (see Supplementary materials). To demonstrate the pH dependence of harvesting by iron oxides, suspension pH was adjusted to 3 using 2 N HCl. At pH 3, it should be noted that iron oxides commonly have positively charged surfaces, described in zeta potential data (see Supplementary materials). As a result, the efficiency of harvesting in the presence of iron oxides increased up to 89.7–89.9% during very short time (~1 min). This observation supports that the electrostatic attraction between the two oppositely charged surfaces largely contributes to aggregating the particles together. On the other hands, the suspension pH was decreased from 9.4 to 4.8 when the culture was purged using ultra-pure CO₂ gas during 5 min, and the harvesting efficiency reached 69.7–70.0% within 1-min agitation time. The decrease in pH can be explained by carbonic acid formation with CO₂ dissolution (CO₂ + H₂O → H₂CO₃). As expected, biomass harvesting at this condition was not superior to that at pH 3, which might be attributed to less positively charged surface of iron oxides at higher pH condition, shown in zeta potential (see Supplementary materials). In addition, compare to the other techniques for harvesting biomass, such as centrifugation or flocculation, it showed lower recovery efficiency (Fasaei et al., 2018). However, this result demonstrated that short-term CO₂ purging with lower operating cost without chemicals input functioned as suspension pH controller in iron oxides-based harvesting system.

3.2. CO₂-supported co-pyrolysis of algae-iron oxides mixture

Three algae samples (MA, MAMH, and MAMH), prepared in the previous step, were transferred to a tubular pyrolytic system. The pyrolytic temperature was increased from 200 to 650 °C at a heating rate of 10 °C min⁻¹ (followed by isothermal 650 °C for 30 min) and the effluent gases were analyzed in real-time, and the evolution profiles of H₂, CO, and CO₂ were shown in Fig. 1. The generation of H₂ from pyrolysis of metal-coupled biomass was initiated at the relatively lower temperature (≥ 440 °C) compared to the case of MA (≥ 480 °C) (Fig. 1a), which supposed that iron oxides could expedite thermochemical degradation of biomass (Du et al., 2020). However, the peak of H₂ production was highest in the MA (0.08 mol% at 600 °C), indicating that the generated H₂ could be consumed in the presence of iron oxides. In other words, the oxidized iron species [Fe(II) & Fe(III)] in mineral phase possibly used H₂ as reductant at high temperature (>420 °C), thereby forming the reduction form of iron (FeO) (Bulavchenko et al., 2019).

On the other hands, the profile of CO evolution showed markedly different output compared to that of H₂ evolution. The enhancement of CO evolution by addition of iron oxides was evident. As shown in Fig. 1b, the formation of CO in the presence of iron oxides was relatively initiated (400 °C) faster than that without any additives (560 °C). Given the previous results that biomass conversion into CO via CO₂-mediated thermal cracking actively started to occur at >500 °C (Kwon et al.,

Table 1
Biomass harvesting efficiencies w/wo physicochemical treatments.

Methods	Iron oxides	pH	Agitation time (min)	Agitation rate (rpm)	Recovery time (min)	Harvesting efficiency (%)	
						MH	MN
No control	X	9.4	- ^a	–	3	3.0±0.3 ^b	
	O	9.4	5	70	3	13.9±0.2	14.3±0.2
	O	9.4	10	70	3	15.6±0.3	15.9±0.1
	O	9.4	30	70	3	17.5±0.2	17.7±0.3
5-min purging of CO ₂	X	4.8	–	–	1	0.4±0.0 ^b	
	O	4.8	1	70	1	69.7±0.2	70.0±0.5
2N HCl injection	X	3	–	–	0.5	6.2±0.1 ^b	
	O	3	1	70	0.5	89.7±0.1	89.9±0.5

^a there was no need for mixing without metal oxide.

^b without iron oxides.

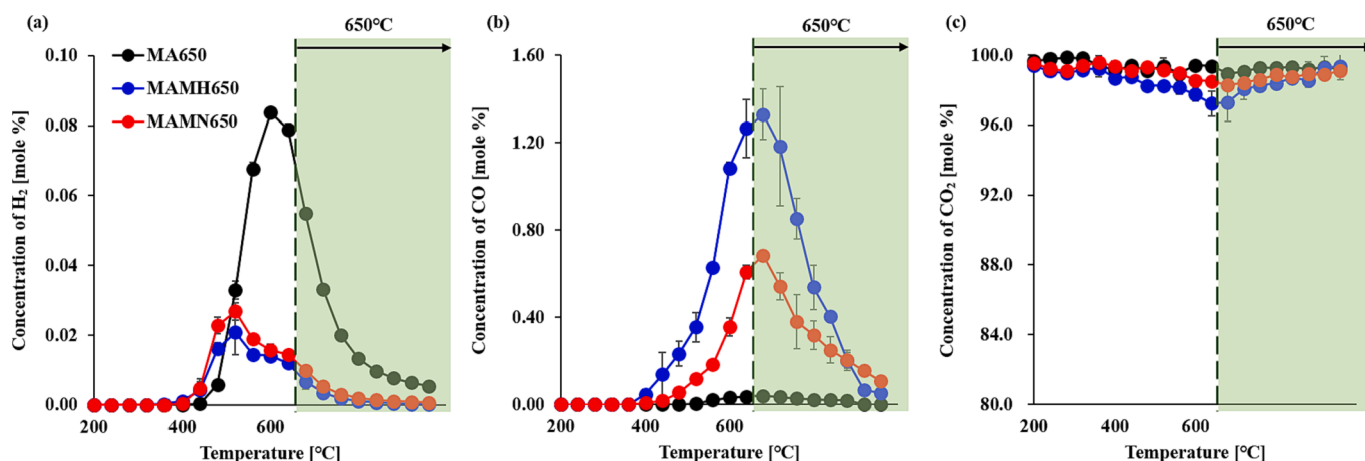


Fig. 1. The evolution profiles of (a) H₂, (b) CO, and (c) CO₂ during co-pyrolysis (feedstock loading = 1 g MA & 1 g MH or MN, heating rate = 10 °C min⁻¹, isothermal pyrolysis time = 30 min).

2022), CO generation at <500 °C was an exceptional case. This observation implies that iron oxides acts as a role of activator in chemically triggering a CO-generating reaction within the temperature range of 400–560 °C. The highest CO formation was achieved by MAMH (1.33 ± 0.12 mol%), followed by MAMN (0.68 ± 0.02 mol%) and MA (0.04 ± 0.01 mol%) at the same temperature of 650 °C. To provide the carbonaceous layers-containing material (*i.e.*, metal-biochar) besides syngas in this work, the final temperature were intentionally lowered to below 710 °C which can thermodynamically facilitate the complete transition of solid carbon to gas via the Boudouard reaction (C + CO₂ → 2CO) (Kwon et al., 2022). Thus, this enhancement cannot be elucidated by the catalytic activity of iron oxides enhancing the Boudouard reaction. In addition, the low level of H₂ production in the presence of iron oxides indicates no outstanding breakdown of biomass to gases. Thus, it is reasonable to assume that iron oxides directly participate in a specific reaction of CO production. Interestingly, MH addition was more effective to generate CO than MN addition in this work. Better formation of CO in the presence of oxygen-rich iron oxides suggests the number of oxygen species present in the mineral phases is closely related to the generation of CO.

According to the previous works (Cho et al., 2019), it has been reported that step-wise reduction of iron phase (Fe₂O₃ → Fe₃O₄ → FeO → metallic Fe) by hydrocarbon gasification in the middle of pyrolytic process occurred as the temperature ranged from 380 to 700 °C. Based on the thermochemical transformation of iron oxides, the presumed reaction pathways of enhancing CO production can be described as follows (see Supplementary materials). First, iron oxides could be

deprived of oxygen to hydrocarbons by iron phase transition through oxygen transfer, and CO might be newly formed during this reaction (Fe₂O₃ + C_xH_yO_z → 2FeO + CO + H₂ + C_{x-1}H_{y-2}O_z). And then, the reduced iron phases might also generate CO by reacting with CO₂ (3FeO + CO₂ → Fe₃O₄ + CO). Thus, oxygen-rich iron oxides (MH) could convert more extent of algae-derived hydrocarbon into CO via sequential phase reduction/oxidation owing to the sufficient extent of lattice oxygen species in MH (Wang et al., 2022).

3.3. Effects of pyrolytic temperature and level of CO₂ feeding on syngas production

To explore the pattern variation in syngas generation influenced by temperature, the effect of pyrolytic temperature on syngas production during co-pyrolysis in CO₂ was investigated by controlling 200 to 450, 550, and 650 °C at a heating rate of 10 °C min⁻¹ (followed by isothermal final temperature for 30 min), and the results were shown in Fig. 2. The generation of H₂ from pyrolysis of MA was proportionally increased with the increase in pyrolytic temperature from 450 to 650 °C, while the addition of iron oxides showed 0.03–0.05 mol% H₂ generation without significant change in the same temperature range (Fig. 2a, 2c, 2e). In general, algae-derived hydrocarbons can be converted into gases at higher temperature (Yang et al., 2019), but the similar level of H₂ in all the temperatures suggests further consumption of H₂ for iron phase transition (*i.e.*, phase reduction) with increasing temperature.

Contrary to the profiles of MA pyrolysis showing no significant variation in CO level, the generation of CO from co-pyrolysis was largely

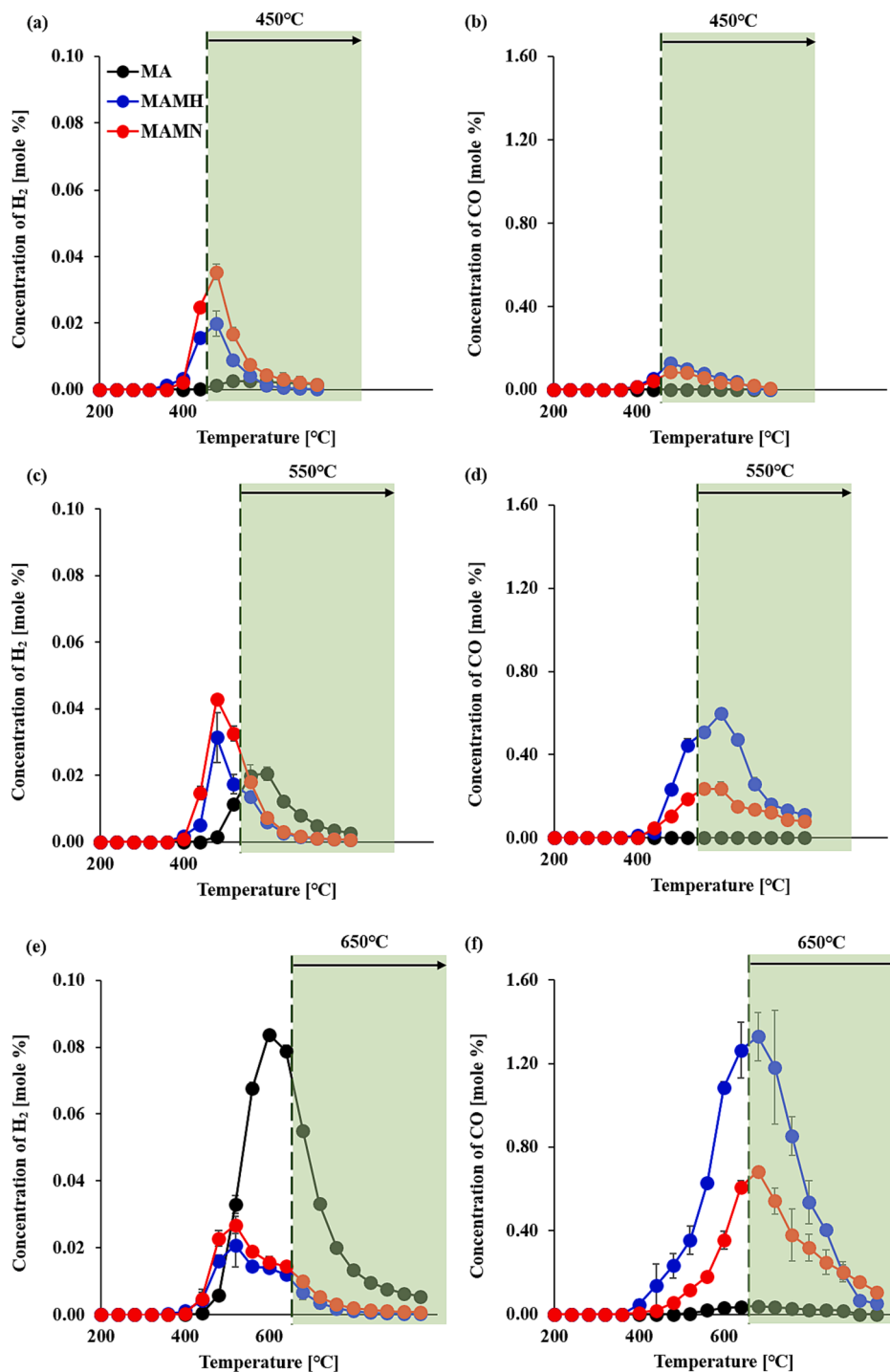


Fig. 2. The evolution profiles of (a, c, e) H₂ and (b, d, f) CO during co-pyrolysis from (a, b) 200 to 450 °C, (c, d) 550 °C, and (e, f) 650 °C (feedstock loading = 1 g MA & 1 g MH or MN, heating rate = 10 °C min⁻¹, isothermal pyrolysis time = 30 min).

impacted by the decrease in pyrolytic temperature from 650 to 450 °C (Fig. 2b, d and f). There was no distinct difference in CO level between MAMH and MAMN, with about 0.1 mol% CO concentration measured in isothermal zone (450 °C) of both samples (Fig. 2b). It turned out that the enhancement in CO production by iron oxides might occur actively at >450 °C. The difference in CO generation between the two samples increased as the temperature rose up to 650 °C (0.60 mol% for MAMH & 0.24 mol% for MAMN at 550 °C, 1.33 mol% for MAMH & 0.68 mol% for MAMN at 650 °C) (Fig. 2d and f). This observation suggests the enhancement by oxygen carrier is highly dependent on the pyrolytic temperature. In addition, previous research suggested that increase of

pyrolytic temperature was conducive to degradation of oxygen-containing functional groups in the feedstock and promoted generation of CO (Lin et al., 2020; Yu et al., 2018). As a result, it could be thought that more oxygen transfer reactions occurring in the presence of MH at higher temperature might lead to further generation of CO via enhanced cracking of hydrocarbons during pyrolysis (Cho et al., 2023; Xu et al., 2021).

Besides CO generation with the phase reduction of iron, however, it should be considered that the phase oxidation by CO₂ also contributes to CO generation. Also, considering the level of CO₂ (~20%) emitted from the sectors (cement, steel etc.), it is desired to use CO₂ at low level in

terms of sustainability as long as CO productivity can be maintained. To examine the susceptibility of reduced iron phase (*i.e.*, FeO), formed after phase reduction, to CO₂ at different level, the experiments were carried out by controlling the level of CO₂ feeding to 0, 20, and 99.999%, and the results were shown in Fig. 3. The initiation temperature of H₂ evolution was similar for each type of biochar samples (≥ 480 –520 °C for MA and ≥ 440 °C for metal-coupled biomass). Interesting note is that the evolution of H₂ was oppositely correlated with the level of CO₂ feeding in the atmosphere. For example, the highest peak of H₂ from MA

pyrolysis was 0.14 mol% at 650 °C under N₂ condition (non-CO₂), while 0.08 mol% H₂ was observed at 650 °C when feeding 99.999% CO₂ (Fig. 3a, 3c, 3e). A previous work has suggested that the injection of CO₂ could induce less formation of aromatic compounds (Lee et al., 2019). Thus, the low substitution of H atoms with alkane molecules in hydrocarbons can elucidate the low level of H₂ generation in the presence of CO₂.

In addition, the outstanding production of H₂ in the presence of iron oxides/N₂ was appeared, with 0.37 mol% H₂ for MAMH at 560 °C &

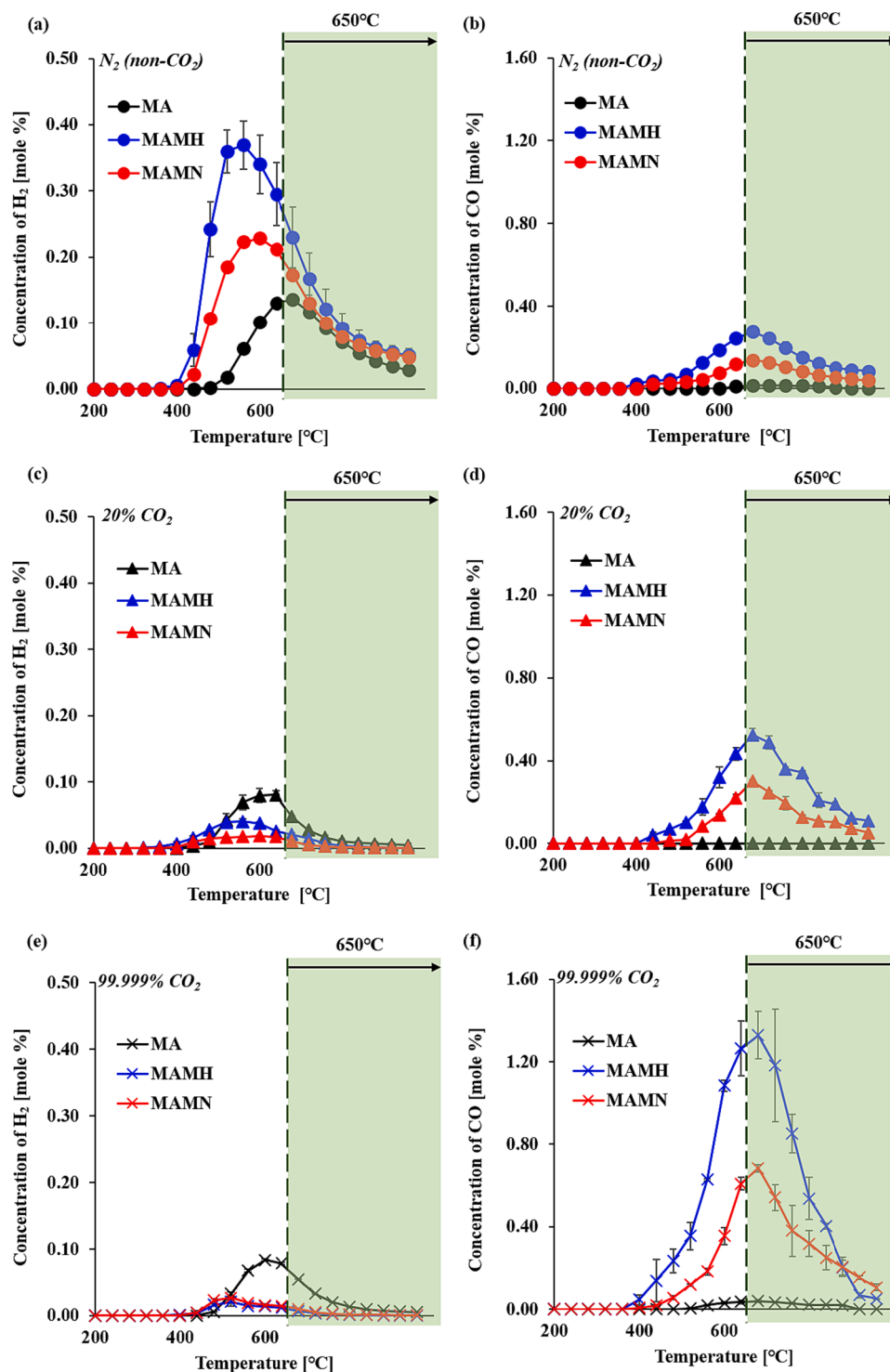


Fig. 3. The evolution profiles of (a, c, e) H₂ and (b, d, f) CO during co-pyrolysis using (a, b) N₂ (non-CO₂), (c, d) 20% CO₂ and (e, f) 99.999% CO₂ as an atmospheric gas (feedstock loading = 1 g MA & 1 g MH or MN, heating rate = 10 °C min⁻¹, isothermal pyrolysis time = 30 min).

0.23 mol% H₂ for MAMN at 600 °C. This observation evidences better cracking of hydrocarbons to gases by oxygen donation of iron oxides as proposed in 3.2 section. However, it was observed that the generation of H₂ in the presence of iron oxides dramatically dropped from 0.23 to 0.37 to below 0.1 mol% when increasing the level of CO₂ feeding to 20%. Compared to iron oxides/N₂ pyrolysis, the lower evolution of H₂ during iron oxides/CO₂ pyrolysis can be explained by consumption of H₂ for Fe₂O₃ or Fe₃O₄ phase reduction to FeO or metallic Fe during pyrolysis.

On the other hands, the highest CO generation was observed in MAMH, followed by MAMN and MA, regardless of injected gas (Fig. 3b, d and f). This observation also evidenced more breakdown of algae-derived hydrocarbons into syngas with the phase reduction by oxygen transfer as suggested above. However, the CO production was highly correlated to the level of CO₂ feeding in the atmosphere, contrary to the H₂ evolution, with the highest peak of CO production observed in 99.999% CO₂ condition among the all prepared samples. For example, the highest peak of CO for MAMH was found to be 0.27 mol% at 650 °C under N₂ condition. When increasing the concentration of CO from 20 to 99.999%, the generation of CO increased from 0.53 to 1.33 mol% at 650 °C. These results supported that the relative concentration of CO₂ in feeding gas remarkably influences CO generation. In other words, the decrease in CO₂ feeding could reduce the susceptibility of reduced iron oxides to CO₂ and then inhibit iron phase oxidation rate, leading to less formation of CO. Given that the generation level of CO in MAMH/20% CO₂ (0.53 mol% at 650 °C) was almost twice as high as that in MAMH/N₂ pyrolysis (0.27 mol% at 650 °C), however, the utilization of CO₂ present in by-product gas could be considered as feeding gas in further study.

3.4. Physicochemical characteristics of metal-biochar

Prior to the application of metal-biochar into toxin removal, the physicochemical properties of metal-biochar were characterized. Three types of metal-biochar samples (MA, MAMH, MAMN) were analyzed by FE-SEM/EDS to explore the surface morphologies and elemental compositions (see Supplementary materials). Compared to the dried sample of MA (before pyrolysis), the morphology of MA biochar showed uneven and irregular surface structure, and the pores formed on its surface were observed. The dried samples of MA aggregated by iron oxides (MAMN & MAMH) exhibited that iron nanoparticles were attached to the surface of algae during harvesting, and the similar morphologies of nanoparticle aggregates were also observed after co-pyrolysis. The EDS data of aggregate surface showed the decrease in C and N contents after pyrolysis for all the biochar samples and the relative increase in O, which can be elucidated by C and N volatilization during thermo degradation of biomass. The interesting observation was that the content of Fe was higher than that of C in the dried samples of MAMN & MAMH prior to pyrolysis, indicating that iron oxides nanoparticles well covered the surface of algae through harvesting. After co-pyrolysis, MAMN & MAMH biochar samples also exhibited the similar elemental contents (low C & high Fe contents).

The N₂ adsorption/desorption isotherm plots of three biochar represented the similar pattern of type II adsorption behavior (see Supplementary materials), which was generally observed in nonporous or macroporous structure (Salaudeen et al., 2018). This observation might be attributed to the absence of lignin in the cell wall of microalgae (Xu et al., 2018). The previous work reported that the presence of lignin in the feedstock could be a critical factor in creating the microporous structure in biochar matrix (Zhang et al., 2022). Thus, less formation of micropores resulted in the relatively low porosity of MA biochar (surface area: 4.4 m²/g, total pore volume: 6 cm³ g⁻¹). Embedding iron oxides nanoparticles into framework was effective to increase the porosity (surface area: 6.7 m²/g for MAMH biochar & 5.4 m²/g for MAMN biochar), but the extent was not large.

The XRD analysis of as-prepared samples was conducted (see Supplementary materials). The XRD spectra of MA generated by three tested

temperature showed relatively indistinct peaks related to the crystallites or metallic components derived from the microalgal biomass or the culture medium (BG-11). However, precise peaks of magnetite (2 θ = 30.2, 35.4, 43.0, 57.1, and 62.6°, JCPDS No. 19-0629) were observed within all the metal biochar samples, describing that the final iron product collected after co-pyrolysis in CO₂ was magnetite. Thus, it was confirmed that magnetite was not further oxidized to oxygen-rich iron oxides in the presence of CO₂. This observation strongly supports the conversion of reduced iron phase into Fe₃O₄ by CO₂ as illustrated in the reaction pathways proposed in 3.2 section.

For better understanding on the carbon nature of metal-biochar, the Raman spectroscopy was analyzed using the same biochar samples used for the XRD analysis (see Supplementary materials). Through the Raman analysis, the two significant peaks (D and G bands) were observed. In general, the intensity ratio of D and G bands (I_D/I_G) represents the disorder degree of carbon structure and lower value of I_D/I_G signifies higher graphitization of carbon (Gao et al., 2019; Kim & Ko, 2020). In this study, the I_D/I_G ratio was correspondingly increased to the final temperature of each biochar, from 0.79 to 0.93 for biochar generated at 450 °C to 1.01–1.16 for biochar generated at 650 °C, which indicated that pyrolytic temperature affected the carbon structural change in biochar (Gabhi et al., 2020; Khiari et al., 2021).

3.5. CO₂-supported toxin removal by metal-biochar

The potential of three types of biochar (MA, MAMH, MAMN)/two types of iron oxides (MH, MN) as an adsorbent for the removal of microcystin from the culture was tested, and the results were shown in Fig. 4. To examine the effect of CO₂ purging on the removal of toxin, the *Microcystis aeruginosa* culture was prepared with or without ultra-high purity of CO₂ purging. First of all, culture pH was significantly dropped from 9.3 to 5.4 by 5-min CO₂ purging, due to the dissolution of CO₂ in the solution. Before adsorption, initial concentration of microcystin was 47.8±3.6 µg/L. There was significant gap of microcystin adsorption capacity of biochar samples according to the support of CO₂ purging (Fig. 4). For comparison, the control without any types of adsorbents was run in parallel, and the microcystin concentration was 82.5±1.5 µg/L after 1 day. This rising of concentration might be related to the cell disruption by mixing stress during adsorption test. However, for instance, the microcystin concentration after adsorption ranged 55.0–60.5 µg/L for three types of biochar under the CO₂ purging condition (Removal efficiency (RE): 27–33%), while 72.9–80.4 µg/L for same adsorbents without purging (RE: 3–14%). A previous work has reported the several potential mechanisms of microcystin adsorption using biochar, such as electrostatic interaction, hydrogen bonding, mesopores filling, hydrophobic interactions and so on (Fristak et al., 2020). The surface charge of microcystin is altered as a function of pH, and therefore the pH of solution has been considered as a major factor for microcystin adsorption (Dixit et al., 2018; Fristak et al., 2020). In general, microcystin is negatively charged at pH 5–6 (Dixit et al., 2018; Serra et al., 2021), while the surface of biochar relatively exhibits positive charge. Therefore, electrostatic attraction between them could enhance the microcystin adsorption capacity of biochar under the relatively acidic pH condition controlled by CO₂ purging. On the other hand, the residual microcystin concentration adsorbed by the iron oxides (76.3 µg/L for MH and 80.4 µg/L for MN) was significantly high compared to the three types of biochar (55.0–60.5 µg/L) under the CO₂ purging condition, although iron oxides might possess positive charge in the range of pH (Markhulia et al., 2021). This observation indicated that the adsorption ability of metal-biochar for microcystin is not mainly dependent on the physicochemical sorption by iron oxides, but carbon layers-driven sorption. In other words, the high removal of microcystin by metal-biochar might be related to the hydrophobic interaction between carbonaceous surface and coiled microcystin under the relatively low pH condition (Fristak et al., 2020). These results suggest that CO₂-supported pH control is remarkably beneficial for microcystin

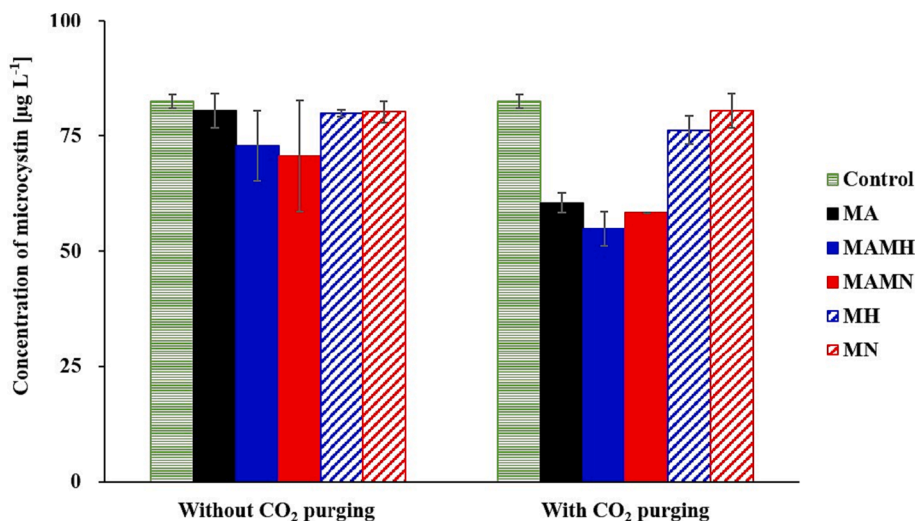


Fig. 4. Concentration of microcystin before and after adsorption test using three types of biochar (MA, MAMH, MAMN) and two types of iron oxides (MH, MN).

adsorption using biochar.

4. Conclusions

Co-pyrolysis of *Microcystis aeruginosa* (MA) and iron oxides, prepared by magnetic harvesting, was performed in CO₂ environment to establish the feasibility of simultaneous production of syngas and metal-biochar. Purging of CO₂ into MA culture functioned as pH controller enhancing magnetic biomass separation (5.0-fold) and adsorption of microcystin (2.8-fold) by metal-biochar. The syngas production (especially CO) was promoted by phase redox reactions of iron oxides inducing CO₂ conversion. These results demonstrated iron oxide and CO₂ utilization for pyrolytic harmful algae conversion performed multiple beneficial. However, by-product gas application as CO₂ supply and toxin removal efficiency should be developed in further study.

CRedit authorship contribution statement

Hyeonjung Yu: Writing – original draft, Investigation, Formal analysis. **Jeong-Yun Jang:** Investigation, Formal analysis. **In-Hyun Nam:** Resources, Funding acquisition. **Hwanju Jo:** Resources, Funding acquisition. **Gil-Jae Yim:** Project administration, Supervision. **Hocheol Song:** Validation, Writing – review & editing. **Dong-Wan Cho:** Conceptualization, Methodology, Investigation, Validation, Writing – review & editing.

Declaration of Competing Interest

The authors declare that they have no known competing financial interests or personal relationships that could have appeared to influence the work reported in this paper.

Data availability

Data will be made available on request.

Acknowledgments

This work was supported by the Korea Environment Industry & Technology Institute (KEITI) through a project for Aquatic Ecosystem Conservation Research Program, funded by the Korea Ministry of Environment (MOE) (2022003040001) and also partly supported by the Korea Institute of Energy Technology Evaluation and Planning (KETEP) grant funded by the Korea government (MOTIE) (20214710100030,

Demonstration of mineral carbonation using FGD gypsum and development of CDM methodology).

Appendix A. Supplementary data

Supplementary data to this article can be found online at <https://doi.org/10.1016/j.biortech.2023.129705>.

References

- Ambaye, T.G., Vaccari, M., van Hullebusch, E.D., Amrane, A., Rtimi, S., 2021. Mechanisms and adsorption capacities of biochar for the removal of organic and inorganic pollutants from industrial wastewater. *International journal of Environmental Science and Technology* 18 (10), 3273–3294.
- Amin, M., Tahir, F., Ashfaq, H., Akbar, I., Razaque, N., Haider, M.N., Xu, J., Zhu, H., Wang, N., Shahid, A., 2022. Decontamination of industrial wastewater using microalgae integrated with biotransformation of the biomass to green products. *Energy Nexus* 6, 100089.
- Ayub, H.M.U., Ahmed, A., Lam, S.S., Lee, J., Show, P.L., Park, Y.K., 2022. Sustainable valorization of algae biomass via thermochemical processing route: An overview. *Bioresour. Technol.* 344, 126399.
- Bulavchenko, O.A., Vinokurov, Z.S., Saraev, A.A., Tsapina, A.M., Trigub, A.L., Gerasimov, E.Y., Gladky, A.Y., Fedorov, A.V., Yakovlev, V.A., Kaichev, V.V., 2019. The Influence of Cu and Al additives on reduction of Iron(III) oxide: In situ XRD and XANES study. *Inorg. Chem.* 58 (8), 4842–4850.
- Chen, W.H., Naveen, C., Ghodke, P.K., Sharma, A.K., Bobde, P., 2023. Co-pyrolysis of lignocellulosic biomass with other carbonaceous materials: A review on advance technologies, synergistic effect, and future prospectus. *Fuel* 345, 128177.
- Cheng, N., Wang, B., Wu, P., Lee, X.Q., Xing, Y., Chen, M., Gao, B., 2021. Adsorption of emerging contaminants from water and wastewater by modified biochar: A review. *EnvironmentPollut.* 273, 116448.
- Cho, D.-W., Chon, C.-M., Yim, G.-J., Ryu, J., Jo, H., Kim, S.-J., Jang, J.-Y., Song, H., 2023. Adsorption of potentially harmful elements by metal-biochar prepared via Co-pyrolysis of coffee grounds and nano Fe(III) oxides. *Chemosphere* 319, 136536.
- Cho, D.W., Yoon, K., Ahn, Y., Su, Y.Q., Tsang, D.C.W., Hou, D.Y., Ok, Y.S., Song, H., 2019. Fabrication and environmental applications of multifunctional mixed metal-biochar composites (MMBC) from red mud and lignin wastes. *Journal of Hazardous Materials* 374, 412–419.
- Choudhary, S., Tripathi, S., Poluri, K.M., 2022. Microalgal-based bioenergy: Strategies, prospects, and sustainability. *Energy & Fuels: An American Chemical Society Journal* 36 (24), 14584–14612.
- Dixit, F., Barbeau, B., Mohseni, M., 2018. Simultaneous uptake of NOM and Microcystin-LR by anion exchange resins: Effect of inorganic ions and resin regeneration. *Chemosphere* 192, 113–121.
- Du, H.B., Deng, F., Kommalapati, R.R., Amarasekara, A.S., 2020. Iron based catalysts in biomass processing. *Renew. Sust. Energ. Rev.* 134, 110292.
- Fasaie, F., Bitter, J.H., Slegers, P.M., van Boxtel, A.J.B., 2018. Techno-economic evaluation of microalgae harvesting and dewatering systems. *Algal Research* 31, 347–362.
- Foong, S.Y., Chan, Y.H., Cheah, W.Y., Kamaludin, N.H., Ibrahim, T.N.B.T., Sonne, C., Peng, W.X., Show, P.L., Lam, S.S., 2021. Progress in waste valorization using advanced pyrolysis techniques for hydrogen and gaseous fuel production. *Bioresour. Technol.* 320, 124299.

- Fristak, V., Laughinghouse, H.D., Bell, S.M., 2020. The use of biochar and pyrolysed materials to improve water quality through microcystin sorption separation. *Water* 12 (10), 2871.
- Gabhi, R., Basile, L., Kirk, D.W., Giorcelli, M., Tagliaferro, A., Jia, C.Q., 2020. Electrical conductivity of wood biochar monoliths and its dependence on pyrolysis temperature. *Biochar* 2 (3), 369–378.
- Gao, R.L., Wang, Q., Liu, Y.H., Zhu, J., Deng, Y.J., Fu, Q.L., Hu, H.Q., 2019. Co-pyrolysis biochar derived from rape straw and phosphate rock: Carbon retention, aromaticity, and Pb removal capacity. *Energy & Fuels: An American Chemical Society Journal* 33 (1), 413–419.
- Geada, P., Oliveira, F., Loureiro, L., Esteves, D., Teixeira, J.A., Vasconcelos, V., Vicente, A.A., Fernandes, B.D., 2019. Comparison and optimization of different methods for *Microcystis aeruginosa*'s harvesting and the role of zeta potential on its efficiency. *Environmental Sciences Pollut.* 26 (16), 16708–16715.
- Hadiya, V., Popat, K., Vyas, S., Varjani, S., Vithanage, M., Gupta, V.K., Delgado, A.N., Zhou, Y.Y., Show, P.L., Bilal, M., Zhang, Z., Sillanpaa, M., Mohanty, S.S., Patel, Z., 2022. Biochar production with amelioration of microwave-assisted pyrolysis: Current scenario, drawbacks and perspectives. *Bioresour. Technol.* 355, 127303.
- Khari, B., Ibn Ferjani, A., Azzaz, A.A., Jellali, S., Limousy, L., Jeguirim, M., 2021. Thermal conversion of flax shives through slow pyrolysis process: in-depth biochar characterization and future potential use. *Biomass Convers.* 11 (2), 325–337.
- Kim, H.B., Kim, J.G., Kim, T., Alessi, D.S., Baek, K., 2021. Interaction of biochar stability and abiotic aging: Influences of pyrolysis reaction medium and temperature. *Chemical Engineering Journal* 411, 128441.
- Kim, D.G., Ko, S.O., 2020. Effects of thermal modification of a biochar on persulfate activation and mechanisms of catalytic degradation of a pharmaceutical. *Chemical Engineering Journal* 399, 125377.
- Kim, Y., Oh, J.I., Vithanage, M., Park, Y.K., Lee, J., Kwon, E.E., 2019. Modification of biochar properties using CO₂. *Chemical Engineering Journal* 372, 383–389.
- Kim, S., Yun, Y.S., Choi, Y.E., 2018. Development of waste biomass based sorbent for removal of cyanotoxin microcystin-LR from aqueous phases. *Bioresour. Technol.* 247, 690–696.
- Kwon, G., Cho, D.W., Jang, H., Lam, S.S., Song, H., 2022. Synergistic effects of blending seafood wastes as Co-pyrolysis feedstock on syngas production and biochar properties. *Chemical Engineering Journal* 429, 132487.
- Lee, T., Oh, J.I., Yi, H., Tsang, Y.F., Kwon, E.E., 2019. Fabrication of carbon-slag composite via a pyrolytic platform and its environmental application for arsenic removal as a case study. *Chemical Engineering Journal* 361, 1630–1639.
- Li, S.X., Hu, T.Y., Xu, Y.Z., Wang, J.Y., Chu, R.Y., Yin, Z.H., Mo, F., Zhu, L.D., 2020. A review on flocculation as an efficient method to harvest energy microalgae: Mechanisms, performances, influencing factors and perspectives. *Renew. Sust. Energy Rev.* 131, 110005.
- Li, X., Liu, B., Lao, Y., Wan, P., Mao, X., Chen, F., 2021. Efficient magnetic harvesting of microalgae enabled by surface-initiated formation of iron nanoparticles. *Chemical Engineering Journal* 408, 127252.
- Lin, J., Ma, R., Luo, J., Sun, S., Cui, C., Fang, L., Huang, H., 2020. Microwave pyrolysis of food waste for high-quality syngas production: Positive effects of a CO₂ reaction atmosphere and insights into the intrinsic reaction mechanisms. *Energy Convers. Manag.* 206, 112490.
- Markeb, A.A., Llimos-Turet, J., Ferrer, I., Blaquez, P., Alonso, A., Sanchez, A., Moral-Vico, J., Font, X., 2019. The use of magnetic iron oxide based nanoparticles to improve microalgae harvesting in real wastewater. *Water Research* 159, 490–500.
- Markhulia, J., Kekutia, S., Mikelashvili, V., Almsay, L., Saneblidze, L., Tsertsvadze, T., Maisuradze, N., Leladze, N., Kriechbaum, M., 2021. Stable aqueous dispersions of bare and double layer functionalized superparamagnetic iron oxide nanoparticles for biomedical applications. *Materials Science - Poland* 39 (3), 331–345.
- Mokhta, Z.M., Ong, M.Y., Salman, B., Nomanbhaya, S., Salleh, S.F., Chew, K.W., Show, P.L., Chen, W.H., 2020. Simulation studies on microwave-assisted pyrolysis of biomass for bioenergy production with special attention on waveguide number and location. *Energy* 190, 116474.
- Salaudeen, S.A., Tasnim, S.H., Heidari, M., Acharya, B., Dutta, A., 2018. Eggshell as a potential CO₂ sorbent in the calcium looping gasification of biomass. *Waste Manag.* 80, 274–284.
- Seo, M.W., Lee, S.H., Nam, H., Lee, D., Tokmurzin, D., Wang, S., Park, Y.K., 2022. Recent advances of thermochemical conversion processes for biorefinery. *Bioresour. Technol.* 343, 126109.
- Serra, A., Philippe, L., Perreault, F., Garcia-Segura, S., 2021. Photocatalytic treatment of natural waters. Reality or hype? The case of cyanotoxins remediation. *Water Research* 188, 116543.
- Singh, G., Patidar, S.K., 2018. Microalgae harvesting techniques: A review. *Journal of Environmental Management* 217, 499–508.
- Vasistha, S., Khanra, A., Clifford, M., Rai, M.P., 2021. Current advances in microalgae harvesting and lipid extraction processes for improved biodiesel production: A review. *Renew. Sust. Energy Rev.* 137, 110498.
- Wang, Y.M., Li, Y., Wang, G.J., Wu, Y.F., Yang, H., Jin, L.J., Hu, S., Hu, H.Q., 2022. Effect of Fe components in red mud on catalytic pyrolysis of low rank coal. *Journal of the Energy Institute* 100, 1–9.
- Weidner, E., Karbassiyazdi, E., Altaee, A., Jesionowski, T., Ciesielczyk, F., 2022. Hybrid metal oxide/biochar materials for wastewater treatment technology: A Review. *ACS Omega* 7 (31), 27062–27078.
- Xu, F., Xing, X., Gao, S., Zhang, W., Zhu, L., Wang, Y., Chen, J., Chen, H., Zhu, Y., 2021. Direct chemical looping gasification of pine sawdust using Fe₂O₃-rich sludge ash as an oxygen carrier: Thermal conversion characteristics, product distributions, and gasification performances. *Fuel* 304, 121499.
- Xu, L., Zhou, M., Ju, H.Y., Zhang, Z.X., Zhang, J.Q., Sun, C.Y., 2018. *Enterobacter aerogenes* metabolites enhance *Microcystis aeruginosa* biomass recovery for sustainable bioflocculant and biohydrogen production. *The Science of the Total Environment* 634, 488–496.
- Yaashikaa, P.R., Kumar, P.S., Varjani, S.J., Saravanan, A., 2019. Advances in production and application of biochar from lignocellulosic feedstocks for remediation of environmental pollutants. *Bioresour. Technol.* 292, 122030.
- Yang, C.Y., Li, R., Zhang, B., Qiu, Q., Wang, B.W., Yang, H., Ding, Y.G., Wang, C.W., 2019. Pyrolysis of microalgae: A critical review. *Fuel Processing Technology* 186, 53–72.
- Yu, K.L., Show, P.L., Ong, H.C., Ling, T.C., Chen, W.H., Salleh, M.A.M., 2018. Biochar production from microalgae cultivation through pyrolysis as a sustainable carbon sequestration and biorefinery approach. *Clean Technologies and Environmental Policy* 20 (9), 2047–2055.
- Zhan, M.M., Hong, Y., 2022. Recent advances in technologies for removal of microcystins in water: a Review. *Curr. Pollut. Rep.* 8 (2), 113–127.
- Zhang, X.Y., Cao, L.Y., Xiang, W., Xu, Y., Gao, B., 2022. Preparation and evaluation of fine-tuned micropore biochar by lignin impregnation for CO₂ and VOCs adsorption. *Sep. Purif.* 295, 121295.
- Zhang, S.Y., Du, X.D., Liu, H.H., Losiewicz, M.D., Chen, X.H., Ma, Y., Wang, R., Tian, Z.H., Shi, L.J., Guo, H.X., Zhang, H.Z., 2021. The latest advances in the reproductive toxicity of microcystin-LR. *Environmental Research* 192, 110254.
- Zhao, C.X., Wang, B., Theng, B.K.G., Wu, P., Liu, F., Wang, S.S., Lee, X.Q., Chen, M., Li, L., Zhang, X.Y., 2021. Formation and mechanisms of nano-metal oxide-biochar composites for pollutants removal: A review. *The Science of the Total Environment* 767, 145305.